5.1. Introduction

The two-dimensional layered nanomaterials, like graphene, graphitic carbon nitride, molybdenum disulfide, tungsten disulfide, and metal-organic frameworks, have numerous research applications because of large specific surface area and weak physical interactions (van der Waals type) existing amongst the adjacent layers.[1–4] These weak interactions furnish outstanding thermal, mechanical, optical, and electrical properties to such nanomaterials.[1] Consequently, their applications have been fully admitted in diverse fields, like catalysis, sensors, photonics, water splitting, energy-storing, hydrogen evolution, and electronics.[1]

Furthermore, for the sustainability of the machine and endurability of its components, 2D nanomaterials have been frequently used as wear and friction-reducing additives to the base lubricating oil.[1-3,5,6] Recently, the tribological properties of some metal selenides such as $MoSe_2$, WSe_2, $NbSe_2$, and monoselenide ZnSe, have been investigated.[7–12] Zhao *et al.* investigated macroscale superlubricity of MoS_2/$MoSe_2$ heterostructures.[13] The lubricating properties of MoS_2 and WSe_2-based nanocomposite coatings were studied by Meister and coworkers.[14] Zhang and associates studied the tribological behavior of ZnSe nanoplates as lubricant additives.[12] The lubricating behavior of $MoSe_2$ hollow nanospheres, nanoflowers, and $MoSe_2$ hybrids with other nanomaterials was studied in detail.[15–17] Zhang and collaborators have shown the tribological applications of the composite of a copper matrix reinforced with Ni/$NbSe_2$.[18] Ultrasound-assisted preparation of $NbSe_2$ micro/nanoparticles and hybrid material was achieved by Qu and coworkers.[10] They tested them for sliding electrical contact as a solid lubricant. The

tribological properties of hexagonal $NbSe_2$ nanoplates were examined by Sun *et al.*[19] Cao and his associates studied the tribological behavior of the tower-like structure of WSe_2 ultrathin nanosheets as an additive to paraffin oil.[9] Besides the above selenides, VSe_2 also holds a layered hexagonal lamellar structure and is well known mainly for hydrogen evolution reactions.[20,21] Li and coworkers tested VSe_2 nanosheets for ultrafast fiber lasers.[22] Investigations on VSe_2 nanosheets for the storage of alkali metal ions were conducted by Ming *et al.*[23] and Yang *et al.*[24]. The nanocomposite of VSe_2 with graphene was used as anode for Li-ion batteries by Wang *et al.*[25], and as cathode material for an aqueous zinc-ion battery by Narayanasamya *et al.*[26] Ghobadi and associates[27] investigated the catalytic properties of VSe_2. $NbSe_2$, VSe_2 being congeners, VSe_2 is expected to be a potential lubricant additive like $NbSe_2$; however, to the best of our knowledge, the tribological properties of VSe_2 have not been explored.

On the other hand, boron-containing compounds in general metal borates, particularly calcium borate,[28] lanthanum borate,[29] and zinc borate are known for their outstanding lubrication behavior. Zinc borate has explicitly been found to be used as an additive to reduce friction and wear. Tian and associates studied the coefficient of friction of nanodisc zinc borate and zinc borate core-shell with SiO_2 nanosphere.[30,31] Zhao and his group exhibited only 14% and 10% reduction in coefficient of friction and wear scar diameter, respectively, using 0.5% zinc borate ultrafine powder in sunflower oil employing a pin-on-disc tribotester.[32] They also investigated lubricating properties of the same without and with surface modification in liquid paraffin oil. They found that wear scar diameter (WSD) increases with zinc borate powder compared to base oil alone;

however, WSD decreases after surface modification.[33] The tribological investigations of chemically capped nanocomposites of zinc borate with MoS_2 (ZB/MoS_2) and graphene oxide (2.0 wt.% of ZB/GO) were achieved by Wu et al.[34] and Cheng et al.[35], respectively. It was noted that the friction coefficient of ZB/GO reduced remarkably compared to ZB/MoS_2, while the opposite trend was observed for wear reduction. Dong and coworkers studied the friction-reducing and antiwear properties of the nano zinc borate with dispersing agent sorbitol monostearate in paraffin oil. They observed an almost 50% drop in coefficient of friction and 10% in WSD.[36]

Further, it has been reported that the tribological functioning under a ravenous condition can be enhanced by improving the lubricating oil-storage capability of the system.[37,38] In the case of porous G-Ni composite, it has been noted that the porosity adds to lubrication behavior in oil.[39] Xiao *et al*. have observed improved mechanical and tribological properties of porous metallic cubic boron nitride reinforced with graphene nanoparticles.[40] The lubrication properties of porous alumina ceramic matrix have been significantly facilitated by immersing polymethyl methacrylate (PMMA)/poly alpha olefins (PAO6) microcapsules.[41]

Additionally, the mechanical property of zinc borate glass has been improved by lanthanum doping.[42] It has been reported that varying concentrations of lanthanum doping have triggered the dosimetric character and thermo-luminescence of zinc borates.[43,44] The enhancement in tribological properties of doped nanomaterials, like magnesium doped zinc oxide, ceria doped zirconia, lanthanum-doped yttria, has been reported from our laboratory.[45,1,5] Furthermore, the composites of the doped

nanomaterials with layered materials like graphene, graphitic carbon nitride, molybdenum disulfide, and copper phthalocyanine have been proclaimed from our group to manifest exemplary tribological behavior.[1,3,5,6]

Considering the above, it engrossed us to synthesize nanoporous zinc borate (ZB), lanthanum doped zinc borate (LZB), lamellar vanadium selenide (VSe_2), and use the synthesized VSe_2 to reinforce LZB (LZB/VSe_2) for upgrading its tribological behavior. Accordingly, VSe_2 nanosheets, ZB, LZB, and LZB/VSe_2 were synthesized, and their tribological activity was appraised in paraffin oil (PO) on a four-ball tester machine under ASTM D4172 and ASTM D5183 conditions.

5.2. Experimental Section

5.2.1. Preparation of additives

5.2.1.1. Preparation of nanoporous zinc borate and La-doped zinc borate

The syntheses of zinc borate and 10% lanthanum-doped zinc borate were brought about by the auto combustion route. For the preparation of zinc borate, $Zn(NO_3)_3 \cdot 6H_2O$ (4.1g), citric acid (3.184 g), and borax (5.08 g) were mixed in distilled water (100 mL) in a beaker and heated at nearly 210 °C with continuous stirring until a gel was produced that turned into black powder. Black powder was calcined at 500 °C for 3 h in a muffle furnace, producing zinc borate. Lanthanum-doped (10%) zinc borate was prepared in the same way using $La(NO_3)_3 \cdot 6H_2O$ (0.367 g), $Zn(NO_3)_3 \cdot 6H_2O$ (2.34 g), borax (3.32 g), and citric acid (2.0 g).

5.2.1.2 Preparation of VSe_2 nanosheets

VSe_2 nanosheets were prepared hydrothermally.[46] 10 mmol SeO_2 (2.22 g), 5 mmol

NH_4VO_3 (1.17 g), and 150 mL distilled water were mixed and stirred for 15 min followed by dropwise addition of 25 mL HCOOH with continuous stirring for 10 min. The contents were shifted into a Teflon autoclave of 200 mL capacity and kept in an oven at 200 °C for 24 h. The collected mixture was cooled down to ambient temperature, filtered and washed through ethanol and deionized water 5-7 times, and then dried at 70 °C to get bulk VSe_2 powder. The bulk VSe_2 powder was exfoliated by ultrasonication for 2 to 3 h in a 50% alcohol-water mixture (200 mL). The dispersion was centrifugated for 20 min at 3500 RPM. The solvent of the supernatant was evaporated to obtain the VSe_2 nanosheets.

5.2.1.3 Preparation of VSe_2 reinforced porous La-doped zinc borate

Vse_2 nanosheets (600 mg) and LZB (400 mg) were taken individually in ethanol (50 mL) and ultrasonicated for 15 min at around 40 °C. The obtained dispersions were mixed and refluxed at 80 °C for 24 h. The resultant colloidal dispersion was filtered and dried at 60 °C. Finally, a grayish-black La-doped zinc borate/lamellar VSe_2 was obtained.

A schematic representation for LZB/VSe_2 synthesis is given in Scheme 1.

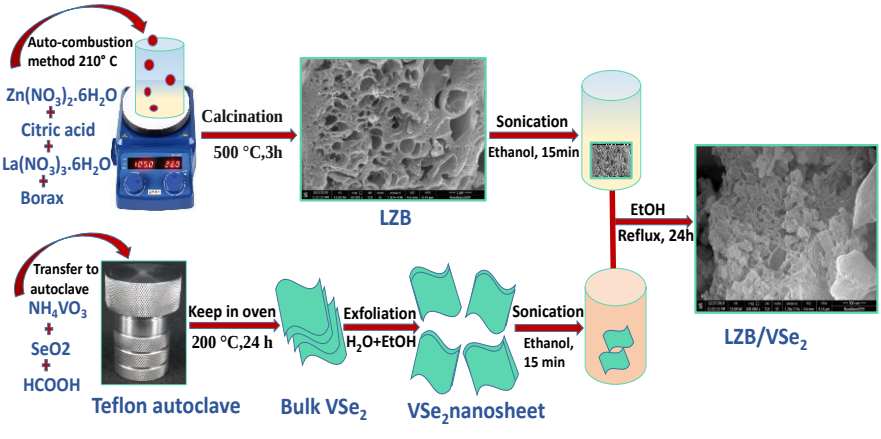

Scheme 5.1. Schematic presentation of synthesis of LZB/VSe_2

5.2.2. Sample preparation

Test samples of different concentrations in the PO, 0.00, 0.10, 0.15, 0.20 and 0.25% w/v were prepared via 1 h sonication at room temperature. The tribological tests were performed at an optimized concentration, i.e., 0.15% w/v in base oil.

5.3. Results and Discussion

5.3.1. Morphological investigation of ZB, LZB, VSe_2, and the LZB/VSe_2

The synthesized additives were studied using XRD, FT-IR, SEM/HR-SEM, TEM/HR-TEM, UV/visible, and XPS. Figure 5.1a reveals XRD patterns of VSe_2, ZB, LZB and LZB/VSe_2. Well-defined diffraction peaks are obtained for VSe_2 nanosheets and assigned to hexagonal structure (JCPDS no. 89-1641).[23] In the diffraction pattern of ZB and LZB, a broad peak at 29.5° is identified for their amorphous structure.[34,35] The heterostructure LZB/VSe_2 did not exhibit any new peaks except those of VSe_2 and LZB. It signifies that VSe_2 nanosheets have efficaciously physically adhered to the surface of LZB, but the intensity of the peaks is considerably reduced.

Figure 5.1b illustrates the IR spectra of the additives. The IR spectrum of ZB shows asymmetric stretching frequencies (υ_{as}) of four and three-coordinate boron at 910 cm^{-1} and 1360 cm^{-1}, respectively, while the symmetric stretching mode (υ_s) of three-coordinate boron is visible at 710 cm^{-1}.[47] However, in the spectrum of LZB, the υ_{as} for four coordinate boron is shifted positively to around 1050 cm^{-1}. The spectrum of VSe_2 is characterized by a peak at 520 cm^{-1} due to υ V-Se, which is identified at approximately 630 cm^{-1} in the LZB/VSe_2.[48] The blue shift of the peak is attributed to the significant interaction of VSe_2 with the LZB.

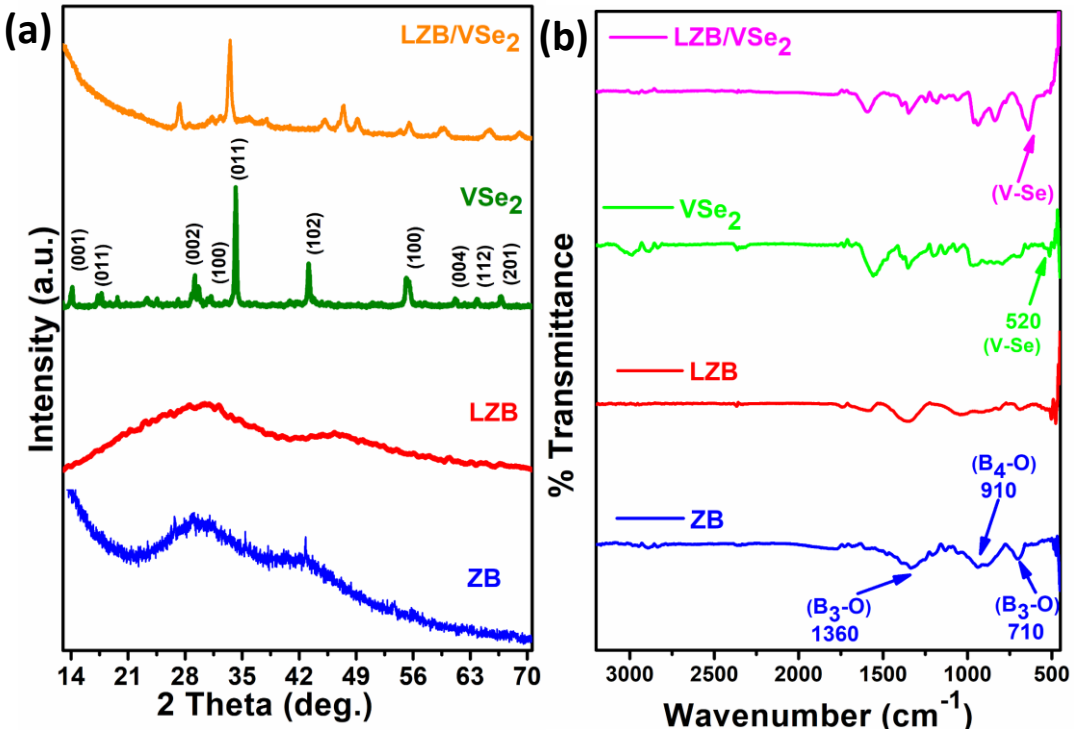

Figure 5.1. (a) XRD patterns of ZB, LZB, VSe_2, and LZB/VSe_2 (b) IR of ZB, LZB, VSe_2, and LZB/VSe_2

The HR-SEM images of ZB, LZB, VSe_2, and LZB/VSe_2 were recorded to inspect their morphologies, Figure 5.2a, 2b, 2c, and 2d, respectively. Randomly assembled fluffy nanosheets of VSe_2 are observable in Figure 5.2a. The lateral measurement of nanosheets lies in the range 100-700 nm with a thickness of 10-70 nm as calculated by Image J software. Figure 5.2b and c discern irregular mesoporous and macroporous structures for ZB and LZB with pores of enormously varying size (4-500 nm) well-scattered throughout. Figure 5. 2d reveals VSe_2 nanosheets spread over and into the pores of La-doped ZB heterostructure depending upon the pore diameter of LZB. The EDX analysis of the LZB/VSe_2, Figure 5.2e, confirms the constituent elements zinc, vanadium,

lanthanum, selenium, boron, and oxygen, endorsing the interaction between LZB and VSe_2. EDX spectra of ZB, LZB, and VSe_2 have been given in Figure 5.3.

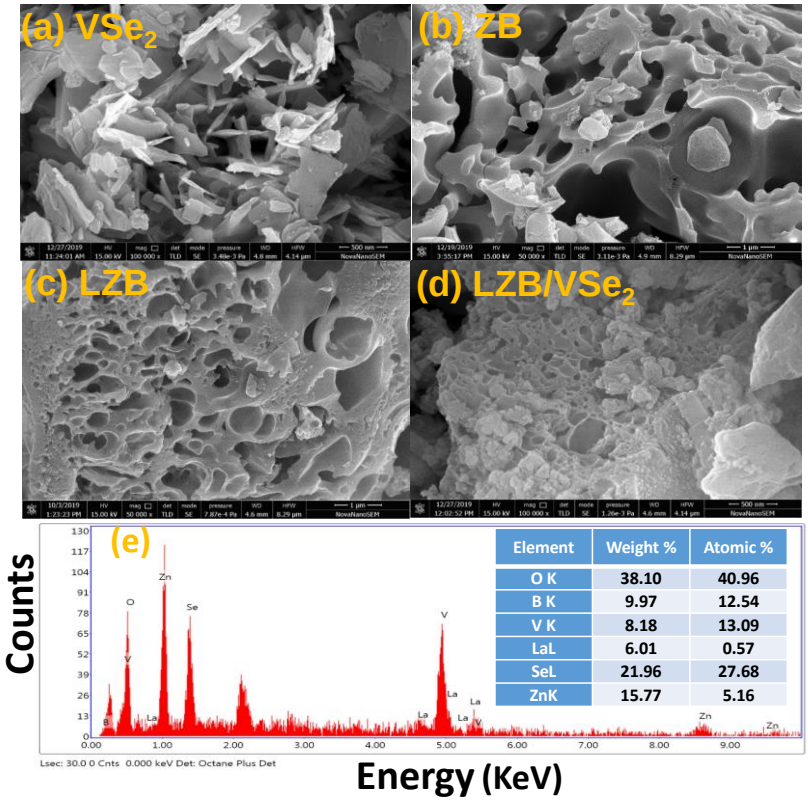

Figure 5.2. HR-SEM images of (a) VSe_2, (b) ZB, (c) LZB, (d) LZB/VSe_2 and (e) EDX spectrum of LZB/VSe_2

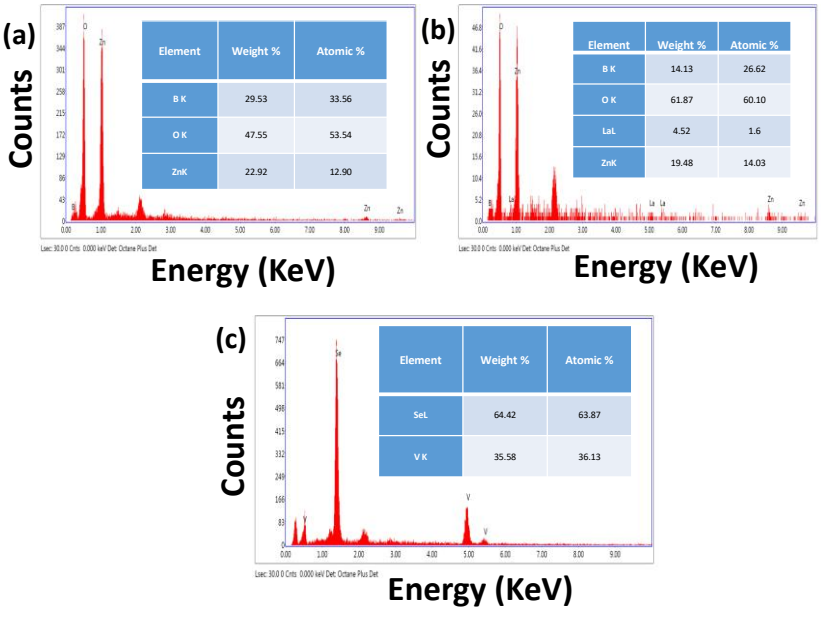

Figure 5.3 EDX spectrum of (a) ZB, (b) LZB, (c) VSe_2

For a more distinct discernment of the morphology, TEM images of vanadium selenide, ZB, LZB, and LZB/VSe_2 have also been documented and are presented in Figure 5.4a, 4b, 4c, and 4d, respectively. In Figure 5.4a, the lamellar structure of VSe_2 is prominently visible with the lattice fringes as 0.26 nm corresponding to the (011) plane.[49] The mesoporous and microporous structures of ZB and LZB can be clearly observed in Figure 5.4b and 4c. The amorphous nature of ZB and LZB can be seen from the selected area diffraction (SAED) pattern, as shown in the inset of the corresponding Figure. Figure 5.4d delineates the anchored VSe_2 nanosheets on porous LZB. The interlayer distance of the VSe_2 nanosheets related to the (011) plane has increased to 0.28 nm in the reinforced structure, as observed in its HR-TEM (Figure 5.4d_1). The increase of the interlayer distance of the (011) plane in VSe_2 nanosheets emphasizes their interaction with the La-doped ZB. The SAED pattern of the reinforced structure, shown in the inset, reveals substantial crystallinity.

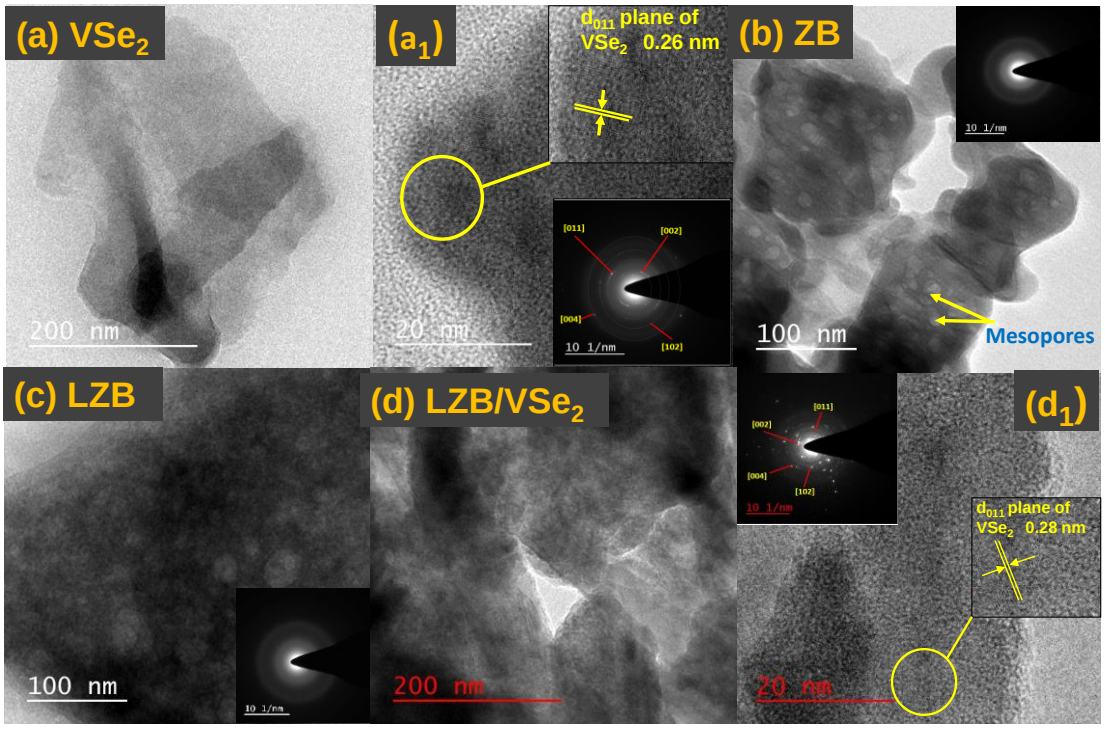

Figure 5.4. TEM photographs of (a) VSe_2, (b) ZB, (c) LZB, (d) LZB/VSe_2 and HR-TEM pictures of VSe_2 (a_1) and LZB/VSe_2 (d_1). The insets in (Fig a_1 and d_1) display the SAED patterns of the additives

The XPS studies could establish the chemical states of the elements in the LZB/VSe_2. The deconvoluted core level spectra of La 3d, Zn 2p, B 1s, O 1s, V 2p, and Se 3d are shown in Figure 5.5 using peak fit software. The core-level spectrum of La 3d reveals peaks at binding energies 834.8 and 838.8 eV conforming to the La^{3+}, Figure 5.5a.[5] The presence of a peak at binding energy 1021.3 eV in the Zn 2p spectrum, Figure 5.5b, corresponds to Zn $2p_{1/2}$ (Zn-O bond).[3,50,51] Figure 5.5c displays two peaks at 188.2 eV and 192.2 eV, indicating the boron oxygen bond.[50,51] The O 1s spectrum, Figure 5.5d, exhibits peaks at 530.2 and 531.6 eV for metal oxides bonds [La-O and Zn-O] and absorbed water, respectively.[3,5] In the core-level V 2p spectrum, the peaks appearing at binding energies

517 eV (V $2P_{3/2}$) and 524 eV (V $2P_{1/2}$), Figure 5.5e, indicate the occurrence of V^{4+} ions.[24] The peak at 53.4 eV corresponds to Se^{2-}.[20,23] in Figure 5.5f.

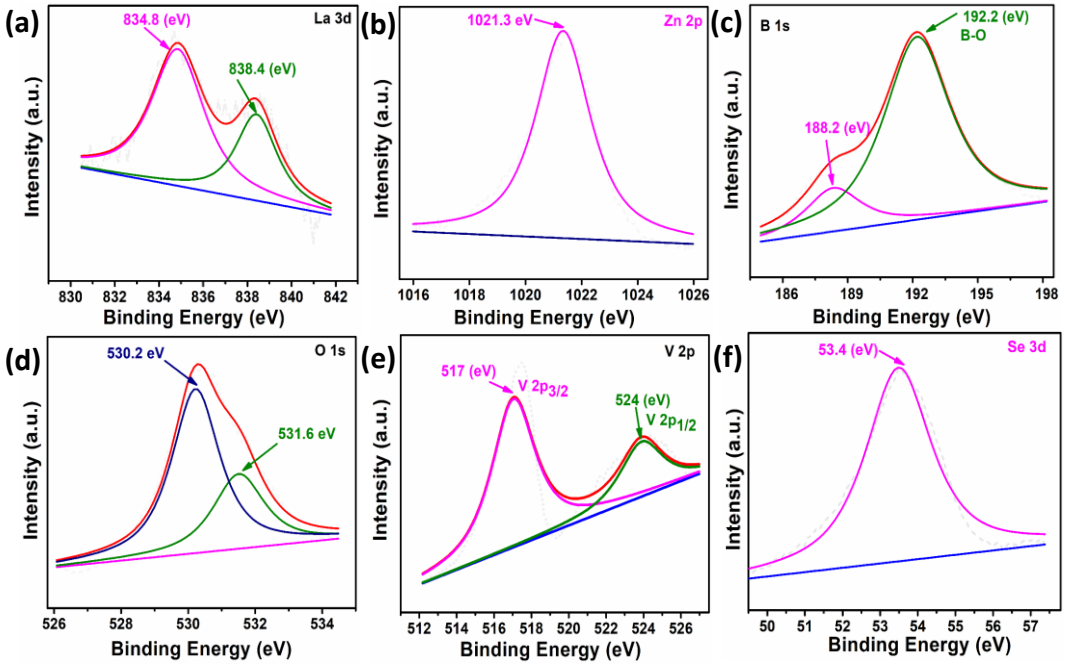

Figure 5.5. Deconvoluted core-level XPS spectra of LZB/VSe_2; (a) La 3d, (b) Zn 2p, (c) B 1s, (d) O 1s (e) V 2p and (f) Se 3d

5.3.2. Tribological behavior of the additives

5.3.2.1. Dispersion Stability of Additives in Base lube

For tribological applications, the dispersion stability of the nanofluids is of particular concern. Electronic spectroscopy (UV/visible) has been helpful for the said objective. The additives (optimized concentration) were ultrasonicated in the base lube and then diluted 10 times. The absorbance data of dilute dispersions were noted down starting from 0 to 48 h. Figure 5.6a displays the plot of relative absorbance of the dispersions versus settling time. The magnitude of reduction in relative absorbance with time relates to the

stability of the dispersion. Apparently, the reinforced structure attains maximum dispersion stability, followed by LZB, ZB, and at last VSe_2.

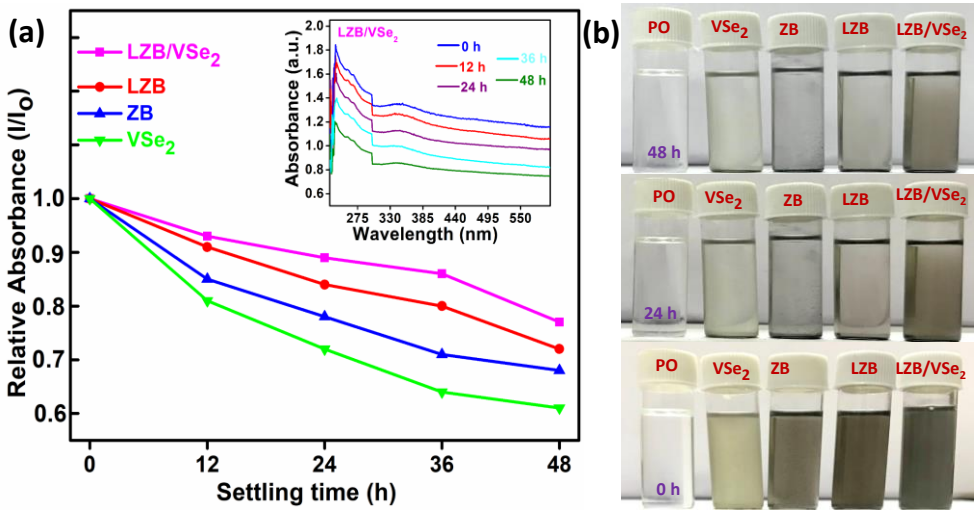

Figure 5.6. (a) Dispersion stabilities of base lube comprising VSe_2, ZB, LZB, and LZB/VSe_2 by UV-vis spectrophotometry, (b) Visual snapshots of the admixtures dispersed in base lube at 0, 24, and 48 h

In the inset of Figure 5.6a, the absorbance values of the LZB/VSe_2 in the beginning and after 24 h and 48 h are displayed at approximately 230 nm. Figure 5.6b presents snapshots of the base lube and the dispersions in the beginning, after 24 and 48 h.

5.3.2.2. Concentration optimization

For describing the efficacy of the additives, the concentration is a vital variant; it must be optimized first. For this, ASTM D4172 standard test (392 N applied load for 60 min at 1200 RPM) was performed in PO with the admixtures in different concentrations, 0.0, 0.10, 0.15, 0.20, and 0.25% w/v and their corresponding mean wear scar diameter (MWD) were noted. A plot of MWD vs. concentration of the additives was drawn, as

depicted in Figure 5,7a. Compared to base lube, values decrease significantly for all the analyzed concentrations of all the additives. Accordingly, wear-reducing behavior is evident at the tested concentrations for all the test materials, but the antiwear efficacies vary extensively. In the case of plain base lube, MWD was noted as 0.735 mm. The relative performance of all additives was found better than the base lube. In general, the MWD reduced up to 0.20% w/v, but beyond that, it rises, excluding the LZB/VSe_2 where MWD rises after 0.15% w/v. Thus, 0.15% of w/v has been taken as the optimized concentration for performing the tests. Variation of MWD in descending order VSe_2 (0.61 mm), ZB (0.545 mm), LZB (0.48 mm), and LZB/VSe_2 (0.426 mm) proves the superiority of the reinforced structure over others.

The optimization of COF vs. additive concentration for each additive is demonstrated in Figure 5.8, showing the minimum antifriction behavior for VSe_2 at (0.15% w/v), ZB (0.2% w/v), LZB (0.2% w/v) and for LZB/VSe_2 (0.15% w/v). Figure 5.7b shows the deviation of coefficient of friction (COF) of the PO alone and its blends with additives vs. time at an optimized concentration of 0.15% w/v. COF is generally relatively greater in each case at the initial stages due to the lack of tribofilm. With the increase of operating time, the COF becomes stable based on *in situ* formed tribofilm. Irregular behavior of COF in the absence of additive has been articulated in the Figure; however, COF is almost uniform when the additives are used. The nature of tribofilm precisely related to the smoothness of the plot. Thus, it is evident that in the case of LZB/VSe_2, tribofilm formed is adherent, homogeneous, and stable.

5.3.2.3. Antiwear and Anti-friction Properties

The ASTM D4172 test was conducted for plain PO and its admixtures with different additives to assess antiwear properties. The outcome of the trial is displayed in Figure 5.7c in the format of a bar diagram wherein both the COF and MWD have been demonstrated conjunctly. It is clear from the graph that the MWD value for PO alone, 0.735 mm, has dropped in each case, showing a % reduction with VSe_2 (18%), ZB (25.86%), LZB (35%), and while LZB/VSe_2 (43%). The drop in MWD is indicative of antiwear efficacy. There is a 9.14% reduction in MWD ongoing from ZB to LZB; thus, La-doping in ZB has improved the activity. The reinforced structure is better efficacious than LZB, while LZB is superior to ZB and VSe_2. The % decrease in average COF value of base lube, 0.079, follows the same pattern as that of MWD; VSe_2 (13%), ZB (41%), LZB (49%), and the LZB/ VSe_2 (69%).

5.3.2.4. Load-carrying ability

At first, the ASTM D5183 test was performed for the optimized concentration of the additives under the following experimental conditions; 392 N load, 600 RPM, temperature 75 ℃, and 60 min to complete the running-in period. After that, the steady-state test is followed by a successive increment of 98 N load at each 10 min cycle until the accomplishment of seizure load due to immediate upsurge of frictional torque, as shown in Figure 5.7d. In the case of base lube, a seizure occurs at the load 1078 N. Subsequently, the adjacent surfaces get seized, and the consequent load is considered the seizure load, signifying the load-carrying capacity of the additive. Physically, the tribofilm is devasted at seizure load, and the lubricant fails to sustain the load. As apparent

from the data, the increase in seizure load of the additives follows their antiwear/antifriction efficiencies; VSe_2 (2040 N), ZB (2138 N), LZB (2327 N), and LZB/VSe_2 (3310 N). Thus, the outstanding load-bearing ability is ostensible for the LZB/VSe_2. The porous structure of LZB in the LZB/VSe_2 accounts for such a high load-bearing ability.

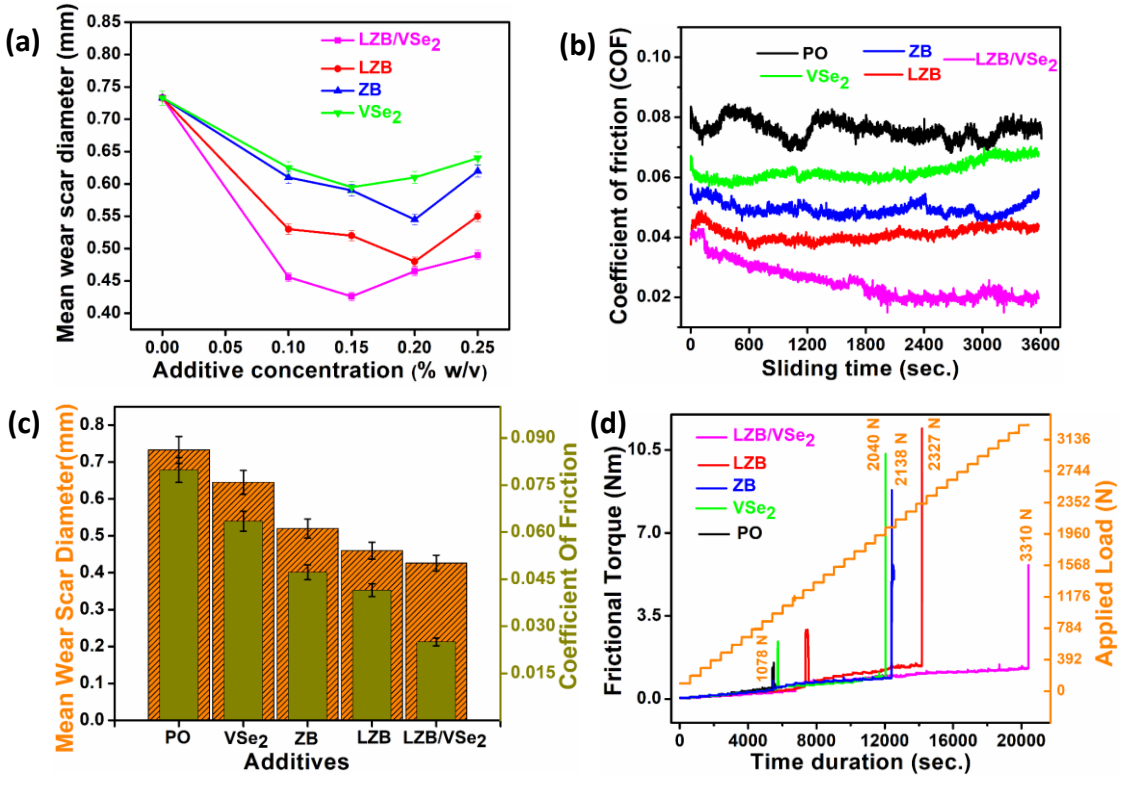

Figure 5.7. (a) ASTM D4172 test results to optimize the concentration of different additives (b) COF against sliding time (c) average coefficient of friction and the MWD in the format of bar diagram (d) frictional torque vs. load and time for plain PO and with different additives under ASTM D5183 standards

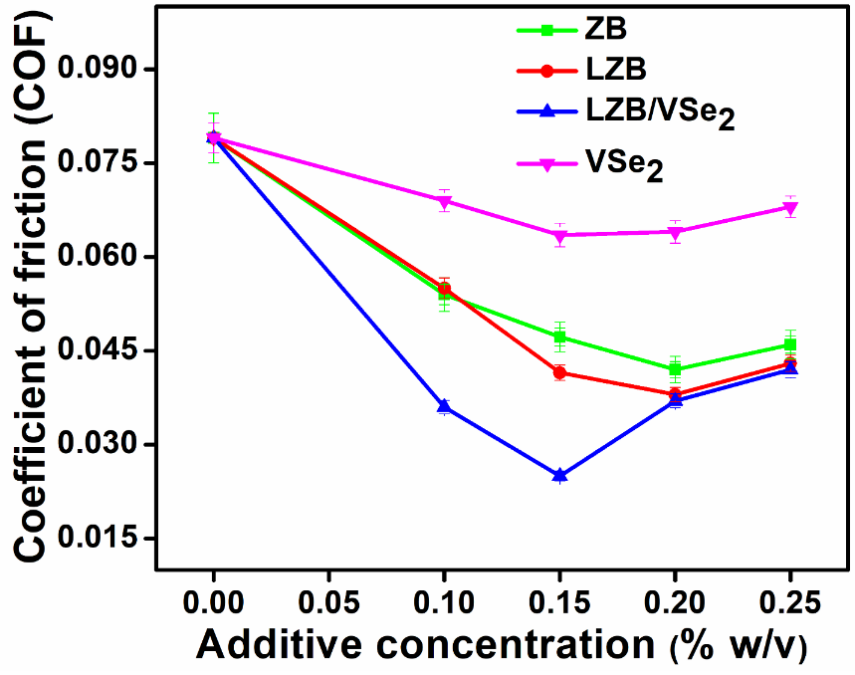

Figure 5.8. Variation of coefficient of friction (COF) vs. additive concentration

5.3.2.5. Frictional Power Loss

The power loss (P) due to frictional force was evaluated for base lube in the presence and absence of the additives using equation (5.1).

$$P = 0.221 \times 3.6 \times \mu \text{ MJ} \quad (5.1)$$

Where μ = coefficient of friction

As mentioned in Table 5.1, for PO alone, very high power consumption (0.0628 MJ) was observed, while there is a significant reduction in power consumption for its blends with various additives; 0.059 MJ for VSe_2, 0.0375 MJ for ZB, 0.033 MJ for the LZB and 0.019 for LZB/VSe_2. Thus, the reinforced structure has minimum power consumption or maximum energy saving.

Table 5.1. Cutbacks in Frictional Power for Individual Additives in PO at the Optimized Concentration, 0.15% (w/v)

	Additives	Power consumption (MJ)	Reduction in Power consumption	% Reduction in Power consumption
1.	PO	0.0628	____	____
2.	VSe_2	0.0590	0.0038	6.00
3.	ZB	0.0375	0.0253	40.30
4.	LZB	0.0330	0.0298	47.45
5.	LZB/VSe_2	0.0190	0.0438	69.74

5.3.3. Morphological Characteristics of Wear Scar Surface

After conducting the antiwear test ASTM D4172, the surface characterization carried out by AFM and SEM assisted in enlightening the morphology of the wear track. The SEM micrographs of the wear track lubricated with PO and its admixture with LZB/VSe_2 (0.15% w/v) are furnished in Figure 5.9.

A furrowed surface due to dreadful scratches for plain PO can be seen in the SEM micrograph; nevertheless, the improved surface is undoubtedly observed in the case of admixtures. The comparative degree of the surface evenness authenticates the results. The evenness of the surface can correlate very well with the MWD values provided in the inset of images. As anticipated, excellent smoothness of the surface is observed when admixture of the LZB/VSe_2 is applied for lubricity. Figure 5.9f shows the EDX analysis

of the wear track, confirming the presence of all elements of the additives, which demonstrates the actively adsorbed additive on the wear track. Boron, as an exception, is usually not identified because of its small size.[6] EDX spectra of the wear pathway of ZB, LZB, and VSe_2 are provided in Figure 5.10.

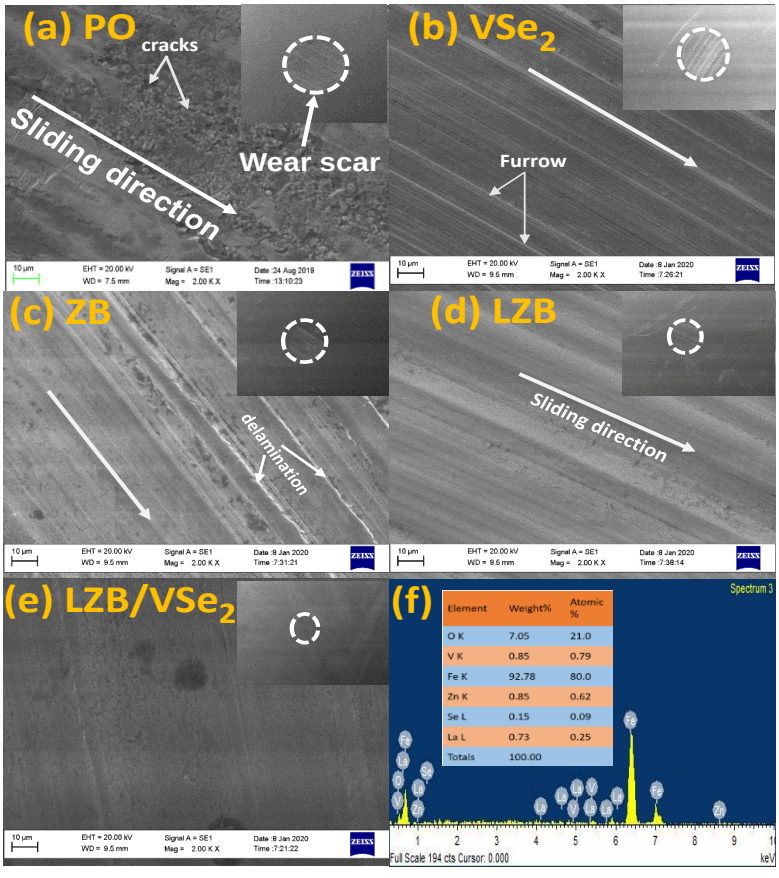

Figure 5.9. (a)-(e) SEM micrographs of the worn surfaces in the presence of PO with and without additives (0.15% w/v) at 2.00 KX amplification under the ASTM D4172 conditions, inset displaying wear scar surface at higher amplification 100 KX (f) EDX spectrum of wear track of steel surface lubricated with LZB/VSe_2

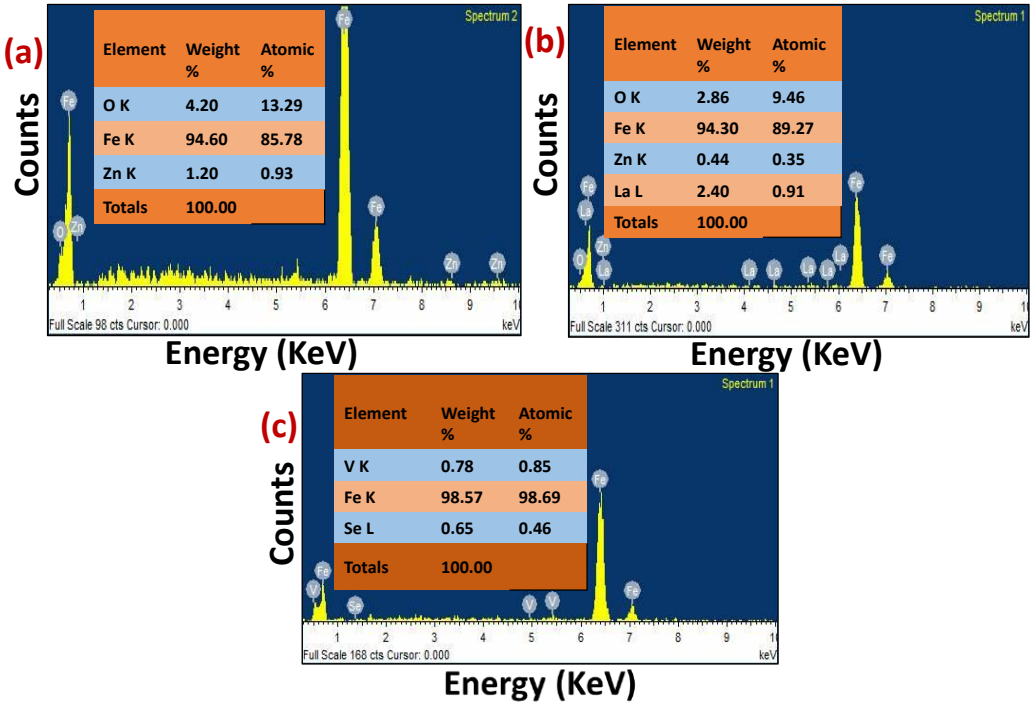

Figure 5.10. EDX spectrum of wear track of steel surface lubricated with (a) ZB, (b) LZB and (c) VSe_2

Furthermore, contact mode AFM was used for plain oil with and without additives to calculate the surface roughness of lubricated steel ball after performing the ASTM D4172 test. Figure 5.11 describes the *3D* and *2D* AFM micrographs of the worn surfaces. The surface roughness values, area roughness (Sq), and line roughness (Rq) related to plain PO and its admixtures are provided in Figure 5.11. Going from base oil to its admixtures, VSe_2, ZB, LZB, and LZB/VSe_2, there is a substantial decline in the Rq and Sq values. As expected, maximum smoothness and slightest roughness are perceived when LZB/VSe_2 is employed as a lubricant additive. Thus, the AFM results validated the evaluations based on SEM analyses. Additional roughness variables like Rm, Ra, Rp, Ry, Rv, Sa, Sy, Sp, Sm, and Sv, have been supplied in Table 5.2.

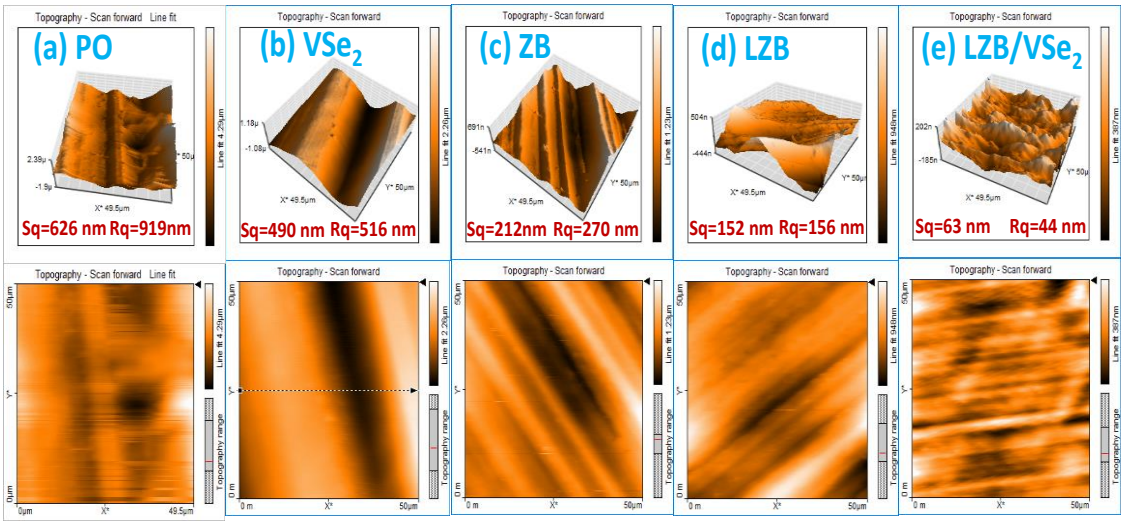

Figure 5.11. *3D* and *2D* AFM images of the wear track lubricated with optimized concentration of blends of additives in PO after conducting ASTM D4172 test, (a) PO, (b) VSe_2, (c) ZB (d) LZB, and (e) LZB/VSe_2

Table 5.2. Surface roughness parameters obtained from the digital processing software of AFM (Nanosurf-basic Scan-2) for different additives after the antiwear test

Surface roughness parameter	Sq (nm)	Rq (nm)	Sa (nm)	Ra (nm)	Sy (nm)	Ry (nm)	Sp (nm)	Rp (nm)	Sv (nm)	Rv (nm)	Sm (pm)	Rm (pm)
PO	626	919	488	771	4363	3255	2611	2060	-1752	-1195	129	-129
ZB	212	270	167	229	1245	977	752	517	-492	-459	162	157
LZB	152	156	118	129	964	565	532	255	-431	-309	145	148
VSe_2	490	516	411	421	2192	1897	1126	964	-1065	-933	136	134
LZB/VSe_2	63	44	49	36	485	194	289	78	-196	-115	108	132

Where, S = Areal roughness, and R = Linear roughness parameters).

Sq = root mean square height, Rq = root mean square line

Sa = Arithmetical mean height, Ra = Arithmetic mean line

Sy = Maximum height of the surface, Ry = Maximum height of the profile

Sp = Maximum peak height**,** Rp = Maximum profile peak height

Sv = Maximum valley depth, Rv = Maximum profile valley depth

Sm = Mean width area, Rm = Mean width line

5.3.3.1. Characterization of Tribofilm by XPS

After ASTM D4172 test, the XPS spectra of the worn surface in the presence of PO alone and blended with LZB/VSe_2 were recorded to examine the chemical states of the constituent elements of the tribofilm generated *in situ*. The deconvoluted core level spectra of La 3d, Zn 2p, B 1s, O 1s, V 2p, Se 3d, and Fe 2p are illustrated in Figure 5.12, employing xps peak fit software.

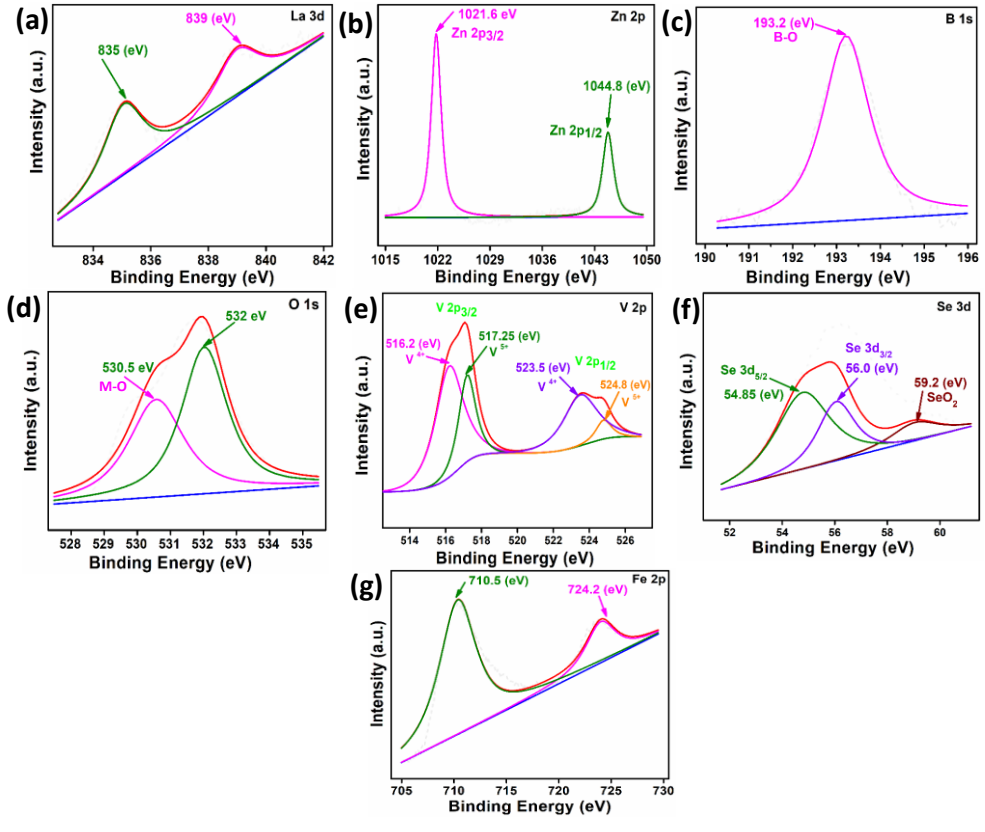

Figure 5.12. Deconvoluted XPS of the tribofilm generated on the wear track in the presence of PO blended with LZB/VSe_2 after ASTM D4172 test (a) La 3d (b) Zn 2p (c) B 1s (d) O 1s (e) V 2p (f) Se 3d and (g) Fe 2p

The position of the peaks in XPS spectra of La 3d, Zn 2p, B 1s, O 1s, V 2p, and Se 3d shows that tribochemical oxidation has resulted in the formation of oxides of lanthanum (La_2O_3), zinc (ZnO), boron (B_2O_3), vanadium (V_2O_5) and selenium (SeO_2). Moreover, the peaks that appear in the Fe 2p XPS spectrum at 710.5 eV (Fe $2p_{3/2}$) and 724.2 eV (Fe $2p_{1/2}$),[12-17] indicate the formation of Fe_2O_3 through the oxidation of Fe of the steel.[2,3,5,6] Thus, the presence of various oxides, particularly ZnO,[3] La_2O_3,[5] B_2O_3,[29] and V_2O_5,[52] usually facilitate lubrication and promote the tribological properties of LZB/VSe_2.

5.3.3.2. Suggested Mechanism of Lubrication

The driving factor for tribological compatibility of the additives relies on their firmness to remain attached over the tribo-surfaces, eventually leading to tribofilm formation during tribological tests, which, in fact, supports the load. The composition, tenacity, and sustainability of the tribofilm are pivotal in understanding the observed efficacy of the additives.

The porous structure of LZB plays a crucial role in enhancing lubricating properties by acting as an intelligent oil reservoir that makes it a self-lubricating system to facilitate the pore structure for discharge of the base oil, which is already stored in pores to the contacting surfaces consistently.[37,38] Meanwhile, through capillary imbibition, it can reuse the additional base oil into the internal pores in between and afterward the work.[38] Thus, the self-lubricating porous LZB shows the benefits of high accuracy, high consistency, and enduring lubrication. Mesopores of LZB fill with only base lube, which is released when required, while the macropores severely affect the mechanical properties because of their merger with the neighbouring ones.[40] The macropores are also filled with

some nanosheets, which are necessary for lower oil consumption. Thus, medium porosity is needed for better consistency of lubrication.[38] The doping of lanthanum has boosted lubrication due to defects. As a consequence of defects, the electronic structure gets affected due to the formation of slip systems, and ultimately, shear strength is diminished.[3]

Undoubtedly, the layered structure of VSe_2 has facilitated the sliding motion due to weak van der Waals forces.[3,5,6] Under thermo-mechanical effects[40] of the tribological test, the nanosheets were squeezed and smeared on the worn surface of the porous LZB matrix due to high contact pressure. The drastic friction at the interface is therefore weakened. The outstanding tribological outcome of LZB/VSe_2 towards minimizing friction, wear, and increasing seizure load may be assigned to cooperative interaction amid the LZB and VSe_2 nanosheets[3,5,6] as depicted in the diagrammatic representation of lubrication mechanism, Figure 5.13. The tribofilm made up of VSe_2 nanosheets on the LZB matrix containing mostly self-lubricating oxides, ZnO, B_2O_3, La_2O_3, V_2O_5 validates the suggested cooperative interaction.

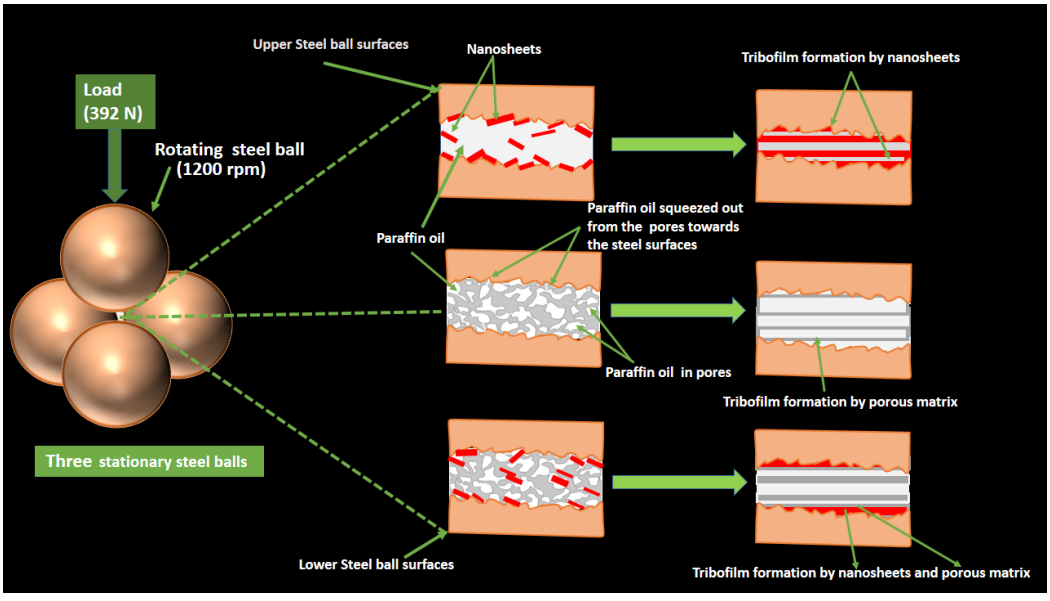

Figure 5.13. The schematic diagram for the suggested mechanism of lubrication

5.4. Conclusions

Nanoporous zinc borate and, La-doped zinc borate were prepared using auto combustion route willfully to take advantage of porosity and doping in enhancing the triboactivity. Assessment of tribological activity by ASTM D4172 and ASTM D5183 tests divulged the effect of porosity and lanthanum doping on the observed results. Hydrothermally prepared VSe_2 nanosheets were used for the furtherance of the tribological activity of LZB. The HR-SEM and TEM studies of LZB/ VSe_2 revealed VSe_2 nanosheets physically adhered to LZB. The as-prepared nanomaterials were characterized by p-XRD, FT-IR, and XPS. Dispersion stability of the blends of nanomaterials in PO was studied by UV/visible spectroscopy. It was found that LZB/VSe_2 was the most stable even after 48 h. The tribological data based on the tests mentioned above for the optimized concentration (0.15% w/v) of the test materials manifest the highest antiwear and antifriction efficiencies of LZB/VSe_2 followed by LZB, ZB, and VSe_2. SEM and AFM

studies of the wear track corroborate the above result. Analysis of the wear pathway by XPS reveals that the tribofilm comprises oxides of La, Zn, V, Se, B, and Fe_2O_3. Doping of La in zinc borate produced defects, further advancing the lubricating properties. Unambiguously, cooperative interaction between LZB and VSe_2 nanosheets governed the commendable tribo-activity of LZB/VSe_2, demonstrating its candidature as aspiring friction and wear modifier for various lubrication systems.

5.5. References

(1) Verma, D. K.; Shukla, N.; Kumar, B.; Singh, A. K.; Shahu, K.; Yadav, M.; Rhee, K. Y.; Rastogi, R. B. Synergistic Tribo-Activity of Nanohybrids of Zirconia/Cerium-Doped Zirconia Nanoparticles with Nano Lamellar Reduced Graphene Oxide and Molybdenum Disulfide. *Nanomaterials* **2020**, *10* (4), 707.

(2) Singh, A. K.; Yadav, A.; Indra, A.; Rastogi, R. B. Superior Performance of Ultrathin Metal Organic Framework Nanosheets for Antiwear and Antifriction Testing. *Colloids Surf. Physicochem. Eng. Asp.* **2021**, *613*, 126100.

(3) Singh, A. K.; Shukla, N.; Verma, D. K.; Kavita; Kumar, B.; Rastogi, R. B. Enhancement of Triboactivity of Nanolamellar Graphitic-C_3N_4 by N-Doped ZnO Nanorods. *Ind. Eng. Chem. Res.* **2021**, *60* (2), 864–874.

(4) Zhang, Y.; Yan, J.; Ren, X.; Pang, L.; Chen, H.; Liu, S. (Frank). 2D WS_2 Nanosheet Supported Pt Nanoparticles for Enhanced Hydrogen Evolution Reaction. *Int. J. Hydrog. Energy* **2017**, *42* (8), 5472–5477.

(5) Shukla, N.; Verma, D. K.; Singh, A. K.; Kumar, B.; Kavita; Rastogi, R. B. Ternary Composite of Methionine-Functionalized Graphene Oxide, Lanthanum-Doped Yttria Nanoparticles, and Molybdenum Disulfide Nanosheets for Thin-Film Lubrication. *ACS Appl. Nano Mater.* **2020**, *3* (8), 8012–8026.

(6) Verma, D. K.; Kuntail, J.; Kumar, B.; Singh, A. K.; Shukla, N.; Kavita; Sinha, I.; Rastogi, R. B. Amino Borate-Functionalized Reduced Graphene Oxide Further Functionalized with Copper Phthalocyanine Nanotubes for Reducing Friction and Wear. *ACS Appl. Nano Mater.* **2020**, *3* (6), 5530–5541.

(7) Li, Y.; Lu, H.; Liu, Q.; Qin, L.; Dong, G. A Facile Method to Enhance the Tribological Performances of $MoSe_2$ Nanoparticles as Oil Additives. *Tribol. Int.* **2019**, *137*, 22–29.

(8) Lu, H.; Chen, L.; Liu, Q.; Li, Y.; Gao, L. Tribological Properties of Biocompatible Molybdenum Selenide Nanoparticles as Water Lubrication Additives for Ultra-High Molecular Weight Polyethylene/304 Stainless Steel Contact. *Mater. Chem. Phys.* **2021**, *272*, 125053.

(9) Cao, K.; Li, C.; Yonghua, C.; Tang, H.; Yan, F.; Song, H.; Yang, X. Graphite-Controlled Fabrication of Ultrathin WSe_2 Nanosheets with Tower-Like Structure and Their Tribological Properties. *Tribol. Trans.* **2012**, *55* (3), 297–301.

(10) Qu, R.; Wen, X.; Zhao, Y.; Wang, T.; Yao, R.; Lu, J. Ultrasonic-Assisted Top-down Preparation of $NbSe_2$ Micro/Nanoparticles and Hybrid Material as Solid Lubricant for Sliding Electrical Contact. *Ultrason. Sonochem.* **2021**, *73*, 105491.

(11) Zhang, F.; Sun, J.; Lu, Y.; Feng, X.; Li, C.; Xu, J.; Tang, G. G. Synthesis and Tribological Properties of $NbSe_2/CeNbO_4$ Nanocomposite. *Mater. Res. Express* **2019**, *6* (9), 095058.

(12) Zhang, X. H.; Xue, M. Q.; Huang, Z. D.; Wang, Z. P.; Yang, F. TRIBOLOGICAL BEHAVIORS OF ZnSe NANOPLATES AS LUBRICANT ADDITIVE. *Chalcogenide Lett.* **2015**, *12* (12), 645-651.

(13) Zhao, Y.; Mei, H.; Chang, P.; Yang, Y.; Huang, W.; Liu, Y.; Cheng, L.; Zhang, L. 3D-Printed Topological $MoS_2/MoSe_2$ Heterostructures for Macroscale Superlubricity. *ACS Appl. Mater. Interfaces* **2021**, *13* (29), 34984–34995.

(14) Domínguez-Meister, S.; Rojas, T. C.; Brizuela, M.; Sánchez-López, J. C. Solid Lubricant Behavior of MoS_2 and WSe_2-Based Nanocomposite Coatings. *Sci. Technol. Adv. Mater.* **2017**, *18* (1), 122–133.

(15) Xue, M. Q.; Wang, Z. P.; Yuan, F.; Luo, G. S.; Zhang, X. H.; Wei, W.; Tang, H.; Li, C. S. TEMPLATE-FREE SYNTHESIS OF $MoSe_2$ HOLLOW NANOSPHERES WITH EXCELLENT TRIBOLOGICAL PROPERTIES. *Chalcogenide Lett.* **2017,** *14* (2), 37-42.

(16) Zhang, X.; Xue, M.; Yang, X.; Luo, G.; Yang, F. Hydrothermal Synthesis and Tribological Properties of $MoSe_2$ Nanoflowers. *Micro Nano Lett.* **2015**, *10* (7), 339–342.

(17) Chen, Z.; Guo, L.; Yan, H.; Yao, H.; Li, L.; Liu, Q. Amino Functionalization of Graphene/Graphene-like $MoSe_2$ Hybrids as Lubricant Additives for Bismaleimide Composites: Preparation, Mechanical and Tribological Properties. *Compos. Part B Eng.* **2019**, *161*, 263–271.

(18) Zhang, F.; Chu, Y.; Li, C. Fabrication and Tribological Properties of Copper Matrix Solid Self-Lubricant Composites Reinforced with Ni/$NbSe_2$ Composites. *Materials* **2019**, *12* (11), 1854.

(19) Sun, J.; Tang, G.; Li, C.; Ji, X.; Liang, W.; Tang, H. Synthesis and Tribological Properties of Hexagonal $NbSe_2$ Nanoplates. *Micro Nano Lett.* **2013**, *8* (6), 294–297.

(20) Yan, M.; Pan, X.; Wang, P.; Chen, F.; He, L.; Jiang, G.; Wang, J.; Liu, J. Z.; Xu, X.; Liao, X.; Yang, J.; Mai, L. Field-Effect Tuned Adsorption Dynamics of VSe_2

Nanosheets for Enhanced Hydrogen Evolution Reaction. *Nano Lett.* **2017**, *17* (7), 4109–4115.

(21) Zhao, W.; Dong, B.; Guo, Z.; Su, G.; Gao, R.; Wang, W.; Cao, L. Colloidal Synthesis of VSe_2 Single-Layer Nanosheets as Novel Electrocatalysts for the Hydrogen Evolution Reaction. *Chem. Commun.* **2016**, *52* (59), 9228–9231.

(22) Li, L.; Pang, L.; Zhao, Q.; Liu, W.; Su, Y. VSe_2 Nanosheets for Ultrafast Fiber Lasers. *J. Mater. Chem. C* **2020**, *8* (3), 1104–1109.

(23) Ming, F.; Liang, H.; Lei, Y.; Zhang, W.; Alshareef, H. N. Solution Synthesis of VSe_2 Nanosheets and Their Alkali Metal Ion Storage Performance. *Nano Energy* **2018**, *53*, 11–16.

(24) Yang, C.; Feng, J.; Lv, F.; Zhou, J.; Lin, C.; Wang, K.; Zhang, Y.; Yang, Y.; Wang, W.; Li, J.; Guo, S. Metallic Graphene-Like VSe_2 Ultrathin Nanosheets: Superior Potassium-Ion Storage and Their Working Mechanism. *Adv. Mater.* **2018**, *30* (27), 1800036.

(25) Wang, Y.; Qian, B.; Li, H.; Liu, L.; Chen, L.; Jiang, H. VSe_2/Graphene Nanocomposites as Anode Materials for Lithium-Ion Batteries. *Mater. Lett.* **2015**, *141*, 35–38.

(26) Narayanasamy, M.; Hu, L.; Kirubasankar, B.; Liu, Z.; Angaiah, S.; Yan, C. Nanohybrid Engineering of the Vertically Confined Marigold Structure of RGO-VSe_2 as an Advanced Cathode Material for Aqueous Zinc-Ion Battery. *J. Alloys Compd.* **2021**, *882*, 160704.

(27) Ulusoy Ghobadi, T. G.; Patil, B.; Karadas, F.; Okyay, A. K.; Yilmaz, E. Catalytic Properties of Vanadium Diselenide: A Comprehensive Study on Its Electrocatalytic Performance in Alkaline, Neutral, and Acidic Media. *ACS Omega* **2017**, *2* (11), 8319–8329.

(28) Huang, Y.; Han, S.; Liu, S.; Wang, Y.; Li, J. Preparation and Tribological Properties of Surface-Modified Calcium Borate Nanoparticles as Additive in Lubricating Oil. *Ind. Lubr. Tribol.* **2014**, *66* (1), 143–150.

(29) Jiang, G. K. C. B. X. M. W. J. F. J. W. Preparation and Tribological Behaviors of Hydrophobic Lanthanum Borate Nanosheets in Rapeseed Oil. *China Pet. Process. Petrochem. Technol.* **2016**, *18* (2), 92.

(30) Tian, Y.; Guo, Y.; Jiang, M.; Sheng, Y.; Hari, B.; Zhang, G.; Jiang, Y.; Zhou, B.; Zhu, Y.; Wang, Z. Synthesis of Hydrophobic Zinc Borate Nanodiscs for Lubrication. *Mater. Lett.* **2006**, *60* (20), 2511–2515.

(31) Tian, Y.; Zhou, W.; Yu, L.; Meng, F.; Yu, K.; Ding, X.; Li, M.; Wang, Z. Self-Assembly of Monodisperse SiO_2-Zinc Borate Core–Shell Nanospheres for Lubrication. *Mater. Lett.* **2007**, *61* (2), 506–510.

(32) Zhao, C.; Jiao, Y.; Chen, Y. K.; Ren, G. The Tribological Properties of Zinc Borate Ultrafine Powder as a Lubricant Additive in Sunflower Oil. *Tribol. Trans.* **2014**, *57* (3), 425–434.

(33) Zhao, C.; Chen, Y. K.; Jiao, Y.; Loya, A.; Ren, G. G. The Preparation and Tribological Properties of Surface Modified Zinc Borate Ultrafine Powder as a Lubricant Additive in Liquid Paraffin. *Tribol. Int.* **2014**, *70*, 155–164.

(34) Wu, P.-R.; Feng, Y.-M.; Ge, T.; Kong, Y.-C.; Ma, Z.-S.; Liu, Z.; Cheng, Z.-L. An Investigation on Tribological Properties of the Chemically Capped Zinc Borate(ZB)/MoS_2 Nanocomposites in Oil. *J. Ind. Eng. Chem.* **2018**, *63*, 157–167.

(35) Cheng, Z.-L.; Li, W.; Liu, Z. Preparation, Characterization, and Tribological Properties of Oleic Diethanolamide-Capped Zinc Borate-Coated Graphene Oxide Composites. *J. Alloys Compd.* **2017**, *705*, 384–391.

(36) Dong, J. X.; Hu, Z. S. A Study of the Anti-Wear and Friction-Reducing Properties of the Lubricant Additive, Nanometer Zinc Borate. *Tribol. Int.* **1998**, *31* (5), 219–223.

(37) Wang, J.; Zhao, H.; Huang, W.; Wang, X. Investigation of Porous Polyimide Lubricant Retainers to Improve the Performance of Rolling Bearings under Conditions of Starved Lubrication. *Wear* **2017**, *380–381*, 52–58.

(38) Wang, C.; Zhang, D.; Wang, Q.; Ruan, H.; Wang, T. Effect of Porosity on the Friction Properties of Porous Polyimide Impregnated with Poly-α-Olefin in Different Lubrication Regimes. *Tribol. Lett.* **2020**, *68* (4), 102.

(39) Lei, Y.; Du, J.; Pang, X.; Wang, H.; Yang, H.; Jiang, J. Tribological Properties and Lubrication Mechanism of in Situ Graphene-Nickel Matrix Composite Impregnated with Lubricating Oil. *Mater. Res. Express* **2018**, *5* (5), 056512.

(40) Xiao, G.; Zhao, B.; Ding, W. Mechanical and Tribological Properties of Porous Metallic CBN Composites Reinforced by Graphene Nanoparticles. *Int. J. Adv. Manuf. Technol.* **2021**, *114* (1), 397–405.

(41) Cheng, Z.; Gong, H.; Wang, Z.; Zhu, L.; Xie, G. Preparation of Self-Lubricating Porous Alumina Ceramics with PMMA/PAO6 Microcapsules and Their Tribological Properties. *Ceram. Int.* **2022**, *48* (6), 8031–8038.

(42) Januchta, K.; Youngman, R. E.; Jensen, L. R.; Smedskjaer, M. M. Mechanical Property Optimization of a Zinc Borate Glass by Lanthanum Doping. *J. Non-Cryst. Solids* **2019**, *520*, 119461.

(43) Kucuk, N.; Kucuk, I.; Cakir, M.; Kaya Keles, S. Synthesis, Thermoluminescence and Dosimetric Properties of La-Doped Zinc Borates. *J. Lumin.* **2013**, *139*, 84–90.

(44) Kucuk, N.; Gozel, A. H.; Yüksel, M.; Dogan, T.; Topaksu, M. Thermoluminescence Kinetic Parameters of Different Amount La-Doped ZnB_2O_4. *Appl. Radiat. Isot.* **2015**, *104*, 186–191.

(45) Verma, D. K.; Kumar, B.; Kavita; Rastogi, R. B. Zinc Oxide- and Magnesium-Doped Zinc Oxide-Decorated Nanocomposites of Reduced Graphene Oxide as Friction and Wear Modifiers. *ACS Appl. Mater. Interfaces* **2019**, *11* (2), 2418–2430.

(46) Xu, K.; Chen, P.; Li, X.; Wu, C.; Guo, Y.; Zhao, J.; Wu, X.; Xie, Y. Ultrathin Nanosheets of Vanadium Diselenide: A Metallic Two-Dimensional Material with Ferromagnetic Charge-Density-Wave Behavior. *Angew. Chem.* **2013**, *125* (40), 10671–10675.

(47) Kipcak, A. S.; Acarali, N. B.; Derun, E. M.; Tugrul, N.; Piskin, S. Low Temperature Solid-State Zinc Borate Synthesis from ZnO and H_3BO_3. *Int. J. Mater. Metall. Eng.* **2013**, *7* (5), 285–289.

(48) Gerlach, C. P.; Arnold, J. Synthesis, Structure, and Reactivity of Three-Coordinate Vanadium(III) Chalcogenolates and Vanadium(V) Chalcogenide Chalcogenolates. *Inorg. Chem.* **1996**, *35* (20), 5770–5780.

(49) Ghobadi, A.; Ghobadi, T. G. U.; Okyay, A. K.; Ozbay, E. Emerging Photoluminescence from Defective Vanadium Diselenide Nanosheets. *Photonics Res.* **2018**, *6* (4), 244–253.

(50) Spadaro, F.; Rossi, A.; Lainé, E.; Hartley, J.; Spencer, N. D. Mechanical and Tribological Properties of Boron Oxide and Zinc Borate Glasses. *Phys. Chem. Glas. - Eur. J. Glass Sci. AndTechnology Part B* **2016**, *57* (6), 233–244.

(51) Li, Y.-M.; Deng, C.; Long, J.-W.; Huang, S.-C.; Zhao, Z.-Y.; Wang, Y.-Z. Improving Fire Retardancy of Ceramifiable Polyolefin System via a Hybrid of Zinc Borate@melamine Cyanurate. *Polym. Degrad. Stab.* **2018**, *153*, 325–332.

(52) Kavita; Singh, A. K.; Shukla, N.; Verma, D. K.; Kumar, B.; Singh, S.; Rastogi, R. B. Polyaniline Intercalated Vanadium Pentoxide Nanosheets for the Improvement of Lubricity of Base Oil. *Colloids Surf. Physicochem. Eng. Asp.* **2022**, *642*, 128644.